AAPS PharmSciTech, Vol. 18, No. 5, July 2017 (© 2016)
DOI: 10.1208/s12249-016-0627-7

Research Article

Design and Evaluation of Novel Solid Self-Nanodispersion Delivery System for Andrographolide

Junnan Xu,[1] Yueqin Ma,[2] Yuanbiao Xie,[1] Yingchong Chen,[1] Yang Liu,[1] Pengfei Yue,[1,3] and Ming Yang[1]

Received 26 June 2016; accepted 29 August 2016; published online 12 September 2016

Abstract. Poorly water-soluble drugs offer challenges in developing a formulation product with adequate bioavailability. This study took advantage of the features of nanocrystals and direct compression technologies to develop a novel solid self-nanodispersion delivery system for andrographolide (Andro) in order to increase its dissolution rate for enhancing bioavailability. Andro nanosuspensions (Andro-NS) with a particle size of about 500 nm were prepared by homogenization technology and further converted into dried nanocrystal particles (Andro-NP) *via* spray-drying. The solid self-nanodispersion delivery system (Andro-SNDS)-loaded Andro-NP was prepared *via* direct compression technology. The DSC and PXRD results demonstrated that the Andro nanocrystals retained its original crystallinity. The dissolution of the Andro-SNDS formulation was 85.87% in pure water over 30 min, better than those of the coarse Andro and physical mixture of Andro and stabilizer. And the C_{max} (299.32 ± 78.54 ng/mL) and $AUC_{0-\infty}$ (4440.55 ± 764.13 mg/L · h) of the Andro-SNDS formulation were significantly higher ($p < 0.05$) than those of the crude Andro (77.52 ± 31.73 ng/mL and 1437.79 ± 354.25 mg/L · h). The AUC of the Andro-SNDS was 3.09 times as high as that of the crude Andro. This study illustrated a novel approach to combine the features of nanocrystals and composite particles used to improve oral bioavailability of poorly soluble drug.

KEYWORDS: andrographolide; bioavailability; nanosuspensions; redispersibility; solid self-nanodispersion delivery system.

INTRODUCTION

In the past two decades, with advances in high-throughput screening, there has been a spiraling increase in the use of active pharmaceutical ingredients. Unfortunately, more than 40% of them are poorly soluble in water, which are thus excluded from further study which is attribute to poor aqueous solubility, or/and poor membrane permeation (1–5). To improve the solubility of such drugs is a major obstacle faced by pharmaceutics scientists (6,7). Nowadays, a well-established and relatively simple strategy to solve this problem is to use particle size reduction. Nanosuspensions (nanocrystal suspensions) are pure particle drug colloidal dispersion systems with a small amount of surfactant or polymer material as a stabilizing agent. Nanosuspensions have some advantages that enhance the saturated solubility and dissolution velocity of poorly soluble drugs owing to their small particle size, reduce fed/fasted state variability, and strengthen the adhesion to biological membrane, prolong adhesion time and detention time, and hence enhance oral bioavailability of drug (8,9). Nanosuspensions are generally produced in water by means of two methods of "bottom up" (such as high pressure homogenization and media milling) and "top down" (including microprecipitation, emulsification, and so on) (10,11). In general, top-down methods are simple and fast to perform, and the process is repeatable and easy to scale up (12). Owing to its physical instability issues, liquid nanosuspensions can be consolidated into dried nanosuspension powders (nanocrystal powders) by means of specialized techniques (spray-drying or freeze-drying) in order to further convert into solid dosage form, namely capsules, granules, and pellets (13). However, a very interesting challenge faced by pharmaceutics scientists is that solid nanosuspension formulations can be reconstituted into the original nanosuspensions before solidification (14).

Andrographolide (Andro, Fig. 1) is a major diterpenoid lactone isolated from *Andrographis paniculata* Nees (Acanthaceae), an herb found in Asian countries such as

Junnan Xu and Yueqin Ma contributed to the work equally as joint first authors.

[1] Key Laboratory of Modern Preparation of TCM, Ministry of Education, Jiangxi University of Traditional Chinese Medicine, 818 Xingwandadao Road, Nanchang, 330004, China.
[2] Departments of Pharmacy, 94th Hospital of People's Liberation Army, Nanchang, China.
[3] To whom correspondence should be addressed. (e-mail: feigleYue@outlook.com)

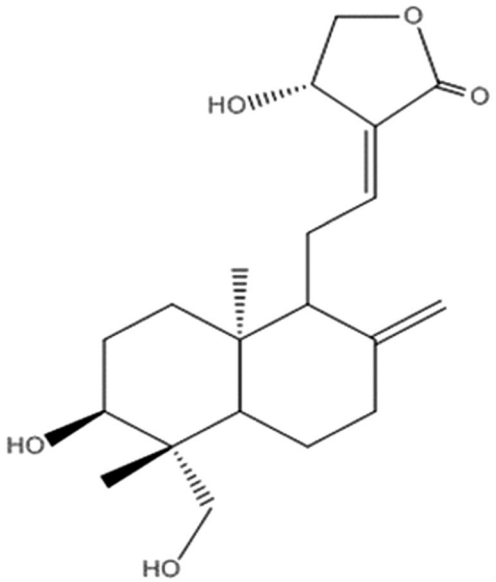

Fig. 1. The chemical structure of Andro

Thailand, India, China, and Southeast Asia, which exhibits a wide range of biological activities including anti-bacterial (15), anti-inflammatory (16), anti-cancer (17), and anti-HIV (18,19). However, Andro is poorly soluble in water (3.29 μg/mL), and has a low oral bioavailability (0.98%) (20,21). Therefore, Andro is a classical BCS II drug (poorly soluble and highly permeable), which means that dissolution is the rate-limiting factor for its absorption. To overcome these issues of Andro, several formulation approaches have been developed, involving the use of drug delivery systems such as solid dispersion (22), cyclodextrin inclusion complexes (23), liposomes (24), and nanoparticles (25). However, the feasibility of commercialization and scale up of these techniques is quite limited.

This study elucidated an attempt to design a formulation strategy of solid self-nanodispersion delivery system-loaded nanosized Andro, with the purpose of enhancing oral bioavailability of Andro. The main objectives of this study were as follows: (1) to prepare Andro nanosuspensions (Andro-NS) and convert it into dried nanocrystal particles (Andro-NP) by spray-drying; (2) to evaluate the particle size and morphology of spray-dried Andro-NP by laser diffractometry and transmission electron microscopy and investigate the solid state of bulk Andro and Andro-NP by means of FTIR, DSC, and XRD analyses; (3) to prepare Andro solid self-nanodispersion delivery system (Andro-SNDS) with excellent redispersibility by powder directly compression technology; and (4) to evaluate the dissolution characterization and oral bioavailability of Andro-SNDS.

MATERIALS AND METHODS

Materials

Andro was purchased from Zelang Co. (Nanjing, China). Microcrystalline cellulose (MCC) was kindly donated by Beijing Fengli Jingqiu Commerce and Trade Co., Ltd. (Beijing, China). TPGS was purchased from Xi'an Healthful Biotechnology (Xi'an, People's Republic of China). Povidone 30 (PVPK30) and Polyplasdone XL10 (PVPP) were kindly donated by ISP (NJ, USA). Lactose was obtained from DAMAO Chemical Co., Ltd. (Tianjin, China). Talc and magnesium stearate were kindly donated by Anhui Sunhere Pharmaceutical Excipients Co. Ltd. (Anhui, China).

Preparation of Andro-NS

Andro-NS was prepared *via* high-pressure homogenization. Before producing Andro-NS, Andro 0.5% (*w*/*v*) and different ratios of PVPK30 and TPGS (*w*/*w*, relative weight to drug) were dispersed in 100 mL water. The obtained mixture was disintegrated into coarse suspension by a high-shear homogenizer (FA25; Fluko, Shanghai, China) at 19,000 rpm for 5 min. Then, the gained coarse Andro suspension was homogenized at predetermined pressure using a piston-gap high-pressure homogenizer (AH-1000D; ATS Engineering, Seeker, Canada). Then, a series of Andro-NCS were obtained. The homogenization conditions and amount of PVPK30 and TPGS were shown in Table I.

Box-Behnken Design

Process of Andro-NS was optimized using 4-factor, 3-level Box-Behnken design using Design Expert® (Version 7.1.6, Stat-Ease Inc., Minneapolis, MN) (26). Results from the preliminary screening trials suggested that the independent values selected were homogenization pressure (*A*, bar), homogenization cycles (*B*, cycles), ratio of TPGS to drug (*C*, %, *w*/*w*), and ratio of PVPK30 to drug (*D*, %, *w*/*w*). The dependent variables were the mean particle size (Y_1, μm) and the span (Y_2). Briefly, the accurately weighed crude Andro was dispersed in different concentrations of stabilizer solution by a high-shear homogenizer. Then, the gained coarse Andro suspension was homogenized at predetermined pressure. A series of Andro-NS with different particles size were obtained. Trials of 29 formulations were carried out according to Table II.

Table I. Process Variables and Their Levels Used in the Box-Behnken Design

	Levels		
	Low	Medium	High
Coded values	−1	0	1
A = homogenization pressure (bar)	600	900	1200
B = cycles	10	20	30
C = amount of surfactant to Andro (*w*/*w*, %)	5	10	15
D = amount of polymer to Andro (*w*/*w*, %)	5	10	15
Dependent variables			
Y_1 = particle size D50 (μm)			
Y_2 = span			

Andro andrographolide

Table II. The Box-Behnken Design and the Corresponding Responded Measurements

Run	*A*	*B*	*C*	*D*	Y_1	Y_2
1	−1	−1	0	0	2.945 ± 0.002	1.216 ± 0.001
2	−1	1	0	0	1.572 ± 0.004	1.062 ± 0.006
3	−1	0	0	−1	2.275 ± 0.001	1.231 ± 0.001
4	−1	0	0	1	2.621 ± 0.003	1.109 ± 0.001
5	−1	0	−1	0	2.413 ± 0.001	1.534 ± 0.001
6	−1	0	1	0	1.143 ± 0.003	1.361 ± 0.005
7	0	0	−1	−1	2.577 ± 0.001	2.038 ± 0.002
8	0	0	1	−1	1.541 ± 0.007	1.733 ± 0.002
9	0	0	−1	1	1569 ± 0.004	1.408 ± 0.001
10	0	0	1	1	0.792 ± 0.001	1.874 ± 0.001
11	0	−1	−1	0	2.253 ± 0.001	2.224 ± 0.001
12	0	1	−1	0	1.056 ± 0.004	1.175 ± 0.001
13	0	−1	1	0	1.887 ± 0.001	2.356 ± 0.001
14	0	1	1	0	0.692 ± 0.001	1.123 ± 0.001
15	0	−1	0	−1	1.709 ± 0.01	1.588 ± 0.006
16	0	1	0	−1	2.009 ± 0.008	1.069 ± 0.005
17	0	−1	0	1	2.157 ± 0.006	2.418 ± 0.006
18	0	1	0	1	0.978 ± 0.003	1.115 ± 0.002
19	0	0	0	0	0.634 ± 0.001	1.329 ± 0.004
20	0	0	0	0	0.652 ± 0.001	1.318 ± 0.003
21	0	0	0	0	0.672 ± 0.002	1.214 ± 0.001
22	0	0	0	0	1.352 ± 0.001	1.472 ± 0.001
23	0	0	0	0	1.319 ± 0.001	1.378 ± 0.002
24	1	−1	0	0	1.024 ± 0.001	2.789 ± 0.001
25	1	1	0	0	0.557 ± 0.004	1.145 ± 0.001
26	1	0	0	−1	0.797 ± 0.007	2.028 ± 0.002
27	1	0	0	1	0.705 ± 0.006	1.738 ± 0.004
28	1	0	−1	0	0.758 ± 0.004	1.534 ± 0.003
29	1	0	1	0	0.687 ± 0.01	1.744 ± 0.005

ANOVA Analysis and Optimization of Model

A statistical model with interactive and polynomial terms was used to evaluate the response values using the formula equation:

$$Y = b_0 + \sum_i b_i x_i + \sum_{ij} b_{ij} x_i x_j + + \sum_j b_i x_i^2 + \sum_{ij} b_{ij} x_i^2 x_j + \sum_{ij} b_{ij} x_i x_j^2 + \sum_j b_i x_i^3 + \varepsilon \quad (1)$$

where y is the response variable, x represents the variables of the system, i and j are design variables, b represents model coefficients that were estimated using a least square fit of the model to the experimental results obtained during the design runs, and ε is the error.

To ensure a desirable model, test for significance of the regression model, test for significance on individual model coefficients, and test for lack-of-fit would be performed, respectively. In order to summarize the tests performed, ANOVA analysis was commonly used. The fitted model is adequate if the model is significant and the lack-of-fit is not significant.

Verification of Optimization Model

According to the results of the optimization model, the predicted optimum values of processes parameters were verified by 5 parallel experiments.

The Particle Size and Span of Andro-NS

The particle size and span of Andro-NS was performed on a Mastersizer Micro Plus (Malvern Instruments Limited, Worcestershire, UK). All measurements were performed in triplicate.

TEM Morphology of Andro-NS

One drop of Andro-NS was placed on a copper grid and stained with 2% phosphotungstic acid solution for 5 min. The grid was dried at room temperature for 12 h and examined using Transmission electron microscope (JEM-1200EX, Japan).

Conversion Andro-NS into Andro-NP *via* Spray-Drying

The Andro-NP was obtained by a Buchi mini spray dryer (model B290, Buchi Laboratoriums-Technik AG, Flawil, Switzerland). The inlet temperature was set as 120°C; aspiration rate, 55%; pump speed, 10%; and atomizing air flow, 50 mmHg. The dried Andro-NP was separated from the drying air in the cyclone (57–83°C outlet temperature). The samples were collected at room temperature for future testing.

Redispersibility of Andro-NP

$$RDI = \frac{D}{D_0} \quad (2)$$

where D_0 is the mean particle size of the freshly prepared Andro-NS before spray-drying and D is the corresponding value of the redispersed Andro-NS from the spray-dried Andro-NP. A redispersibility (RDI) value of near 1 means that Andro-NP can completely reconstituted into the original Andro-NS after rehydration.

Scanning Electron Microscopy

Morphological of the representative samples of Andro-NP powder was examined using scanning electron microscope (SEM) (Nova Nano SEM45, FEI, USA). All samples were placed on conductive double-sided carbon tapes and coated with a thin layer of gold with a sputter coater (Fison Instruments, UK) using an electrical potential of 2.0 kV at 25 mA for 10 min.

Differential Scanning Calorimetry

The thermal properties of the coarse Andro powder, TPGS, PVPK30, MCC, lactose, their physical mixture and

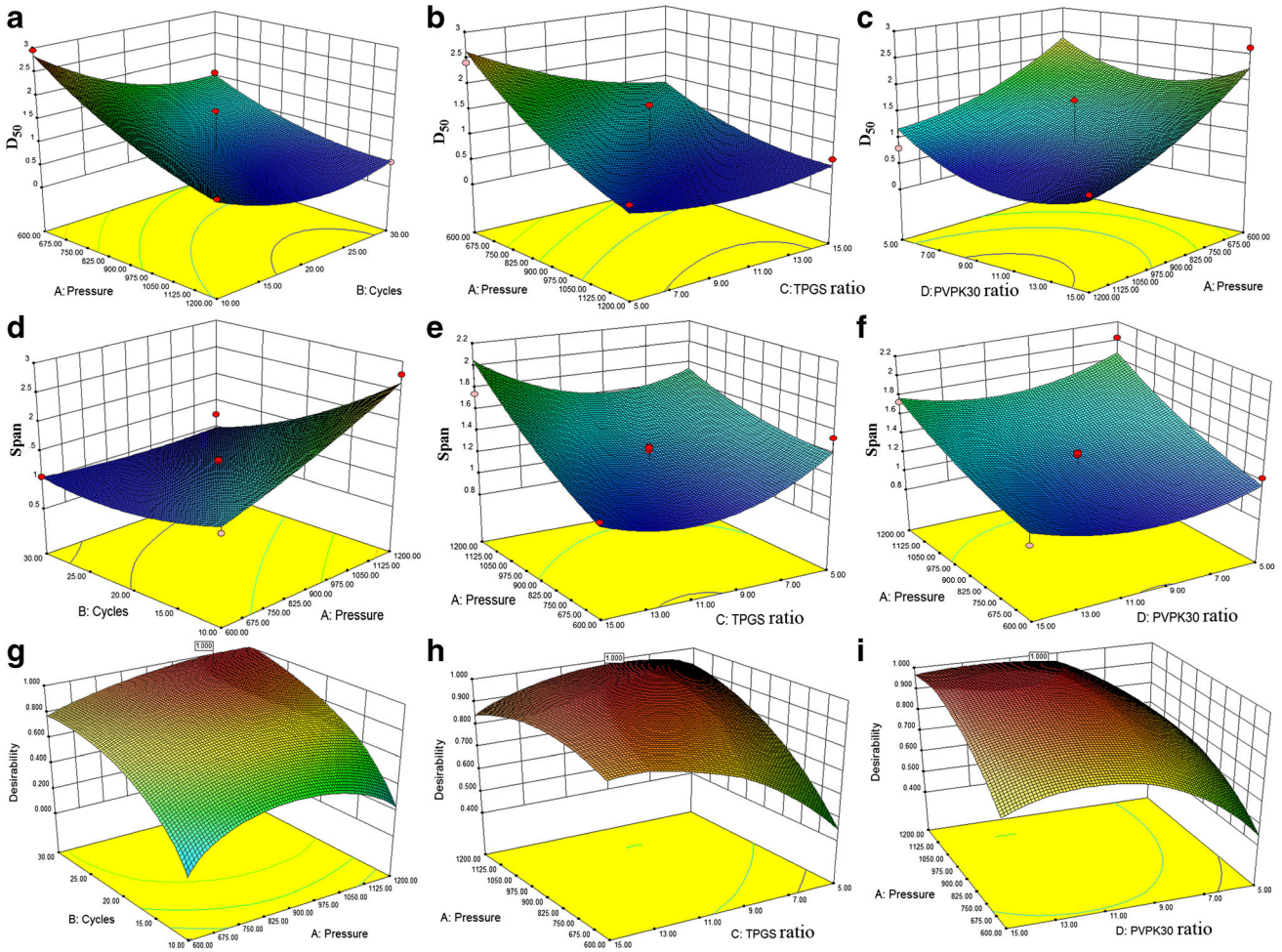

Fig. 2. Fitted surface for response values as a function of the pressure (**a**), homogenization cycles (**b**), ratio of TPGS to Andro (**c**) and ratio of PVPK30 to drug (**d**); the particle size (D50) (**a–c**), the span (**d–f**); and the desirability (**g–i**)

Andro-NS powder were performed using a differential scanning calorimetry (DSC) (Diamond DSC, Perkin-Elmer, USA). Each sample was accurately weighed in pierced aluminum pans and scanned under a nitrogen purge with a heating rate of 10°C/min from 50 to 260°C.

Fourier Transforms Infrared Spectrophotometry

The interaction between Andro, PVPK30, MCC, and lactose in Andro-NP was studied by Fourier transform infrared spectrophotometry (FT-IR Spectrometer, BRUKER IFS-55, Switzerland). The IR spectra of coarse Andro powder, PVPK30, MCC, lactose, their physical mixture, and Andro-NP powder was compressed into thin slice with potassium bromide and scanned over the range 4000 to 400 cm^{-1}, respectively.

Powder X-ray Diffraction

The crystal characterizations of coarse Andro powder, PVPK30, MCC, lactose, their physical mixture, and Andro-NP powder were analyzed by a powder X-ray diffractometer (D8ADVANCE, BRUKER AXS GMBH, German).

Table III. The Mean Particles Size and Span of Spray-Dried Andro-NP Used Different Matrix Formers (Relative Weight to Drug, *w/w*, %), Respectively

Concentration	100% MCC	100% lactose	50%MCC + 50%lactose
D50 (*nm*)	522.49 ± 0.004	514.38 ± 0.003	514.39 ± 0.001
RDI	2.608 ± 0.014	1.015 ± 0.003	1.017 ± 0.001

MCC microcrystalline cellulose, *RDI* redispersibility

Measurements were carried out over from 3° to 90° at a scanning rate 2°/min.

Preparation of Andro-SNDS

Accurately weighed amount of optimized Andro-NP (40%, *w*/*w*) along with MCC (*w*/*w*, 30%) and lactose (*w*/*w*, 20%) were mixed thoroughly. To these mixtures, 8% of PVPP (*w*/*w*), 1% of magnesium stearate (*w*/*w*), and 1% of talc (*w*/*w*) were added and mixed further by means of the mortar. The obtained powder mixtures were directly compressed into tablet (50 mg Andro/tablet) by a rotary tablet compression machine (Mini Press II, Pharmag, Germany).

In Vitro Drug Release of Andro-SNDS

A RC-8 dissolution tester (Tianjin Guoming Medicine and Equipment Co., Inc., China) was used to evaluate the *in vitro* dissolution performance of Andro-NS, Andro-NP, and Andro-SNDS according to the USP Apparatus II method. Samples of Andro, the physical mixture (Andro, PVPK30, and TPGS), Andro-NS, Andro-NP, and Andro-SNDS (equivalent to 60 mg) was dispersed in 900 ml of pure water used as a dissolution medium at 37°C. The rotation speed of the paddles was set at 100 rpm. Two-milliliter samples were withdrawn and filtered through 0.22-μm filter membrane immediately at predetermined time intervals (0.5, 1, 1.5, 4, 6, 10, 20, and 30 min). Simultaneously, equal blank medium was compensated immediately after the withdrawal. The amount of dissolved Andro in the sample solution was determined by HPLC method. The chromatographic separation was achieved on Hypersil ODS2 (250 mm × 4.6 mm, 5 μm) with a Security Guard column (10 × 4.6 mm, 5 μm). The temperature was ambient. The mobile phase consisted of methanol–water (60:40, *v*/*v*). The flow rate was 1 mL/min. The detection wavelength was set at 225 nm and the injection volume was 20 μL.

In Vivo Pharmacokinetic Study of Andro-SNDS

The study was approved by the Institutional Ethics Committee of Jiangxi University of Traditional Chinese Medicine. Male Wister rats with an average weight of 200 ±

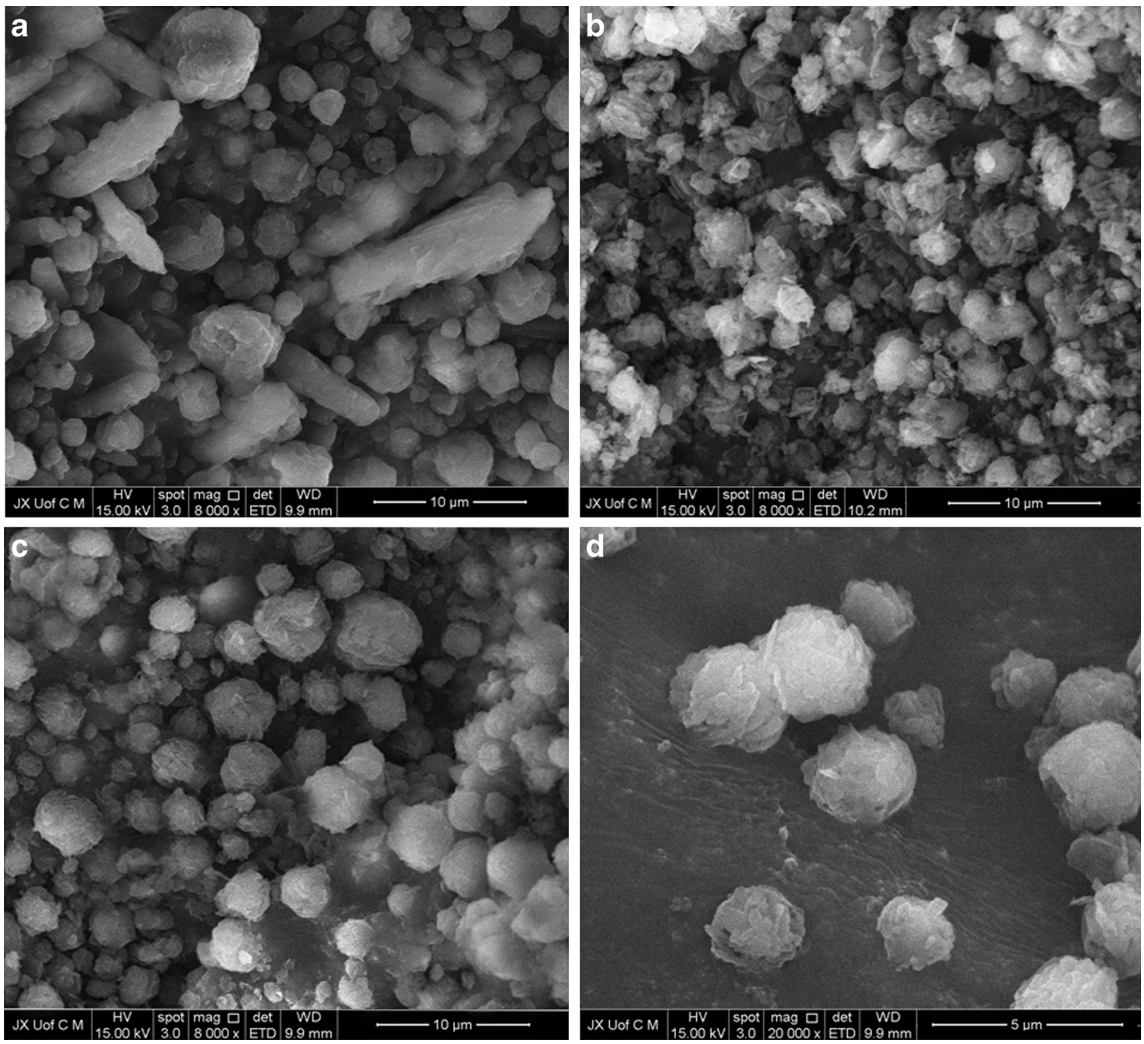

Fig. 3. SEM morphology of Andro-NP. **a** Andro-NP/MCC (×8000), **b** Andro-NP/lactose (×8000), **c** Andro-NP/MCC + lactose (×8000), **d** Andro-NP/MCC + lactose (×20,000)

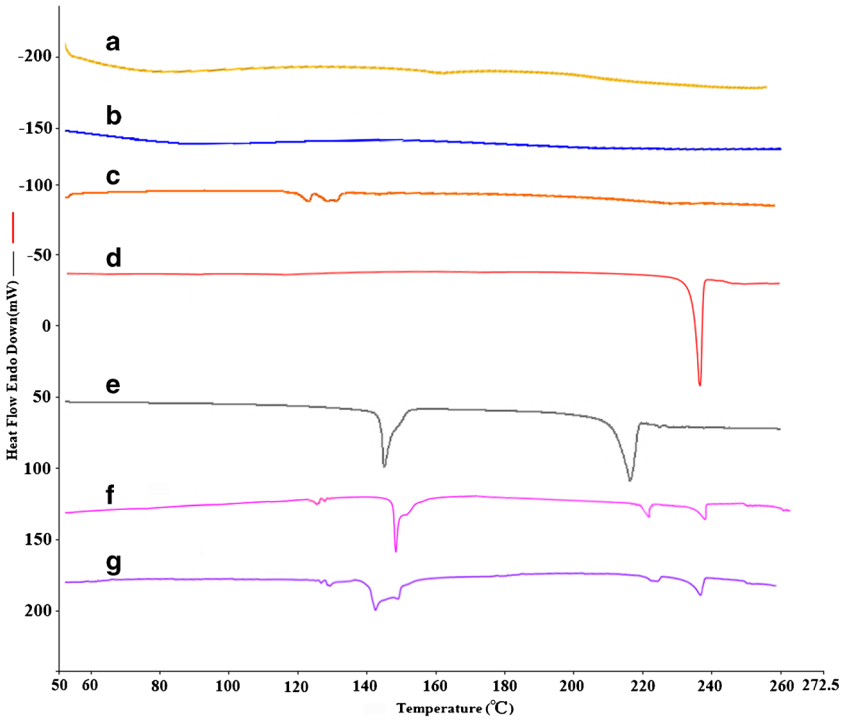

Fig. 4. DSC thermograms of PVPK30 (**a**), MCC (**b**), TPGS (**c**), raw Andro (**d**), lactose (**e**), the physical mixture (**f**), and the spray-dried Andro-NP powders (**g**)

20 g were randomly divided into two groups ($n = 6$). The rats were fasted for 12 h prior to the study and all groups were given a single oral dose of 10 mg/kg Andro (24). At the predetermined intervals 0.25, 0.5, 1, 1.5, 2, 3, 4, 6, 9, 12, 15, and 24 h, the blood sample of 0.25 ml was collected by retro orbital puncture, respectively. Plasma was obtained from whole blood in heparinized tube by centrifugation at 4000 rpm for 15 min and was frozen at −20°C until analysis. A validated HPLC/MS/MS system was used to determine the Andro plasma concentrations (25,27). Carbamazepine was used as internal standard (IS). The full scan spectra showed parent ion at m/z 349.10 for Andro and m/z 237.0 for IS, respectively. An elution system of acetonitrile:water (5:95, v/v) was used with a flow rate of 0.3 ml min^{-1}. The retention times for Andro and IS were 2.86 and 4.5 min, respectively.

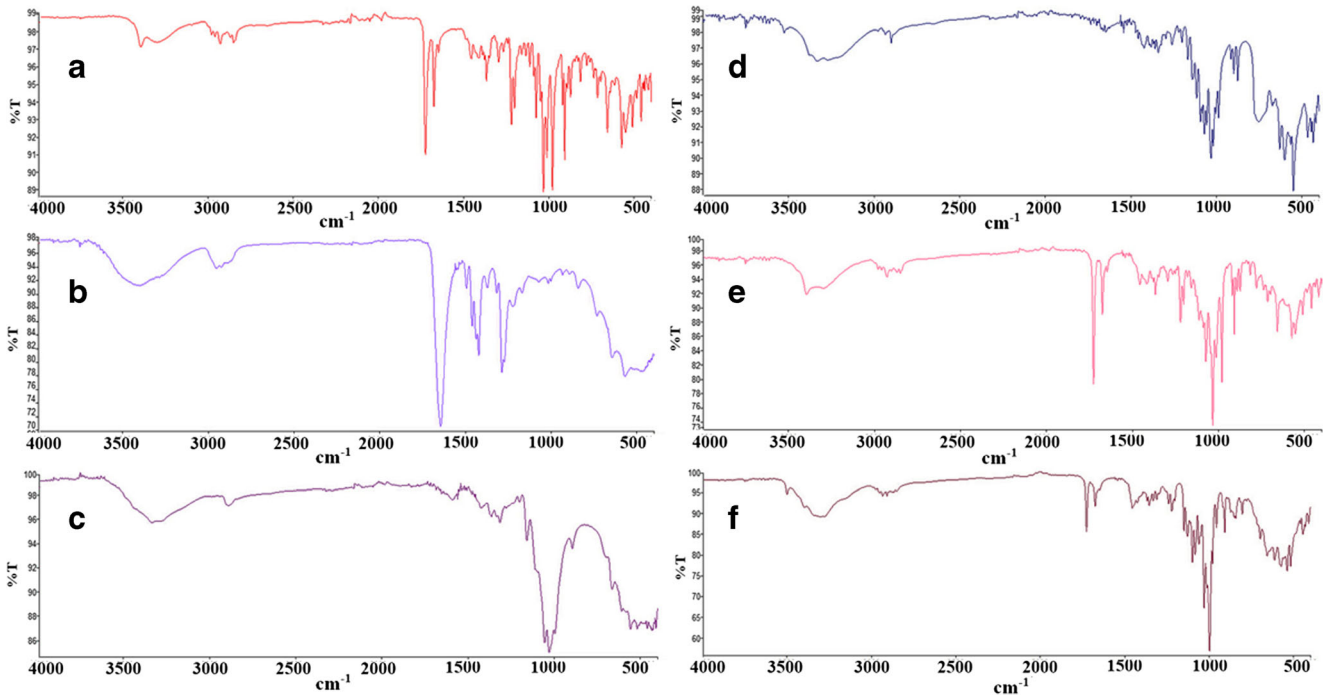

Fig. 5. FT-IR analysis of raw Andro (**a**), PVPK30 (**b**), MCC (**c**), lactose (**d**), the physical mixture (**e**), and the spray-dried Andro-NP powders (**f**)

Statistical Analysis

The main pharmacokinetics parameters were processed and obtained by DAS 2.0 software (Mathematical Pharmacology Professional Committee of China). ANOVA analysis was carried out using IBM SPSS Statistics 21 software. Differences were considered statistically significant if the p value was less than 0.05.

RESULTS

Process Optimization of Andro-NS via Box-Behnken Design

Table II shows the experimental conditions of the Box-Behnken design with the corresponding values observed for the two response values. Experimental data was fitted to the quadratic model by ANOVA analysis. The results indicated that all the three models were significant at 95% confidence and the lack of fit was not significant. The fitted models in terms of coded factors were Eqs. (3)–(4). Coefficient of determination (R^2) for particle size and span was 0.8674 and 0.8832, respectively.

Figure 2a–f shows that surface response graphs for the effects of the predetermined factors on the measured response values.

$$Y_1 = 1.10 - 0.70A - 0.43B - 0.32C - 0.17D + 0.05AB - 0.37BD + 0.33B^2 + 0.25C^2 + 0.44D^2 \quad (3)$$

$$Y_2 = 1.28 + 0.31A - 0.48B - 0.35AB + 0.18B^2 + 0.26C^2 + 0.19D^2 \quad (4)$$

Effect of Matrix Formers on Redispersibility of Andro-NP During Spray-Drying

Table III shows that the mean particle size and RDI of Andro-NP stabilized by different concentrations of lactose and MCC. It could be seen that the Andro-NP used 100% concentration of lactose and 50% of MCC + lactose as matrix formers possessed excellent redispersibility, respectively. But the Andro-NP used 100% MCC as matrix formers had formed some irreversible aggregation (RDI 2.408) during spray-drying. These could also be seen from the microscopic images of Andro-NP (Fig. 3).

Differential Scanning Calorimetry

Figure 4 shows that thermal behavior of PVPK30, MCC, TPGS, raw Andro, lactose, the physical mixture (Andro + PVPK30 + TPGS + MCC + lactose), and the spray-dried Andro-NP powders. As it can be seen, PVPK30 and MCC did not show sharp endothermic peak in the investigated range. Lactose showed endothermic peaks at 140 and 220°C. TPGS exhibited an endothermic peak at 130°C. Raw Andro and physical mixture exhibited the same melting peak at 240°C. The thermal characterizations of the physical mixture showed a combination effect of Andro, PVPK30, TPGS, MCC, and lactose (Fig. 4a–e).

Fourier Transforms Infrared Spectrophotometry

Figure 5 shows that the infrared spectra of Andro, MCC, PVPK30, lactose, the physical mixture (Andro + PVPK30+ MCC + lactose), and the spray-dried Andro-NP. The following characteristic absorption peak of Andro could be seen: OH, 3200–3400 cm^{-1}; C=CH_2, 1 671 cm^{-1}, 907 cm^{-1}; and Δαβ-γ-lactone, 1731 cm^{-1} (Fig. 5a). The spectrum of the physical mixture showed a combination effect of Andro, PVPK30, TPGS, MCC, and lactose (Fig. 5a–d). It was also seen that the spectrum of spray-dried Andro-NP (Fig. 5f) was not significantly different with those of the physical mixture (Fig. 5e).

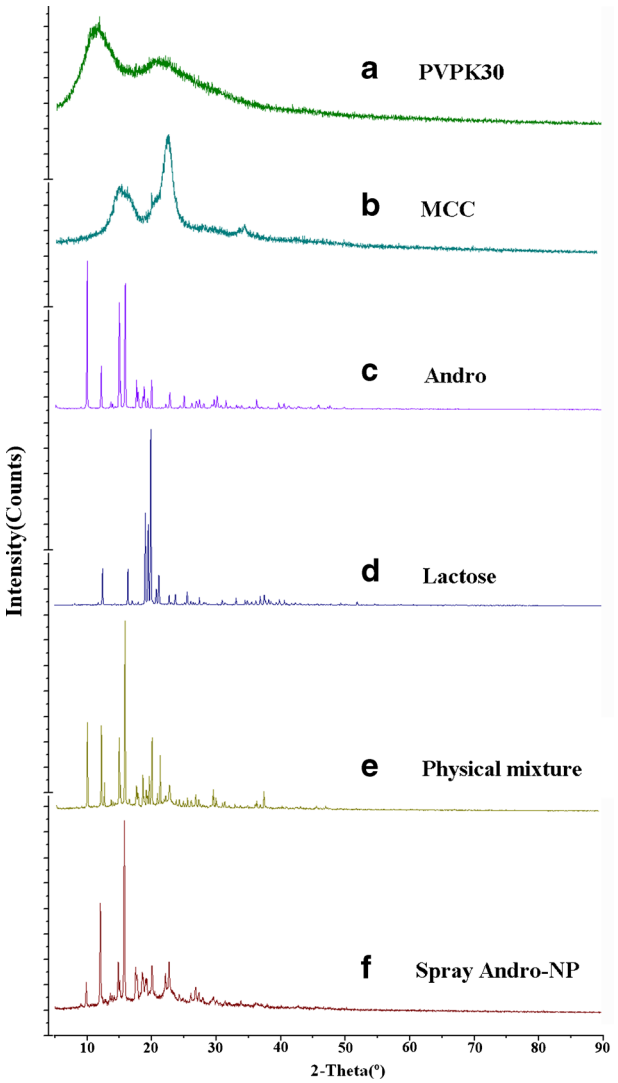

Fig. 6. XRD diffractograms of PVPK30 (**a**), MCC (**b**), TPGS (**c**), raw Andro (**d**), lactose (**e**), the physical mixture (**f**), and the spray-dried Andro-NP powders (**g**)

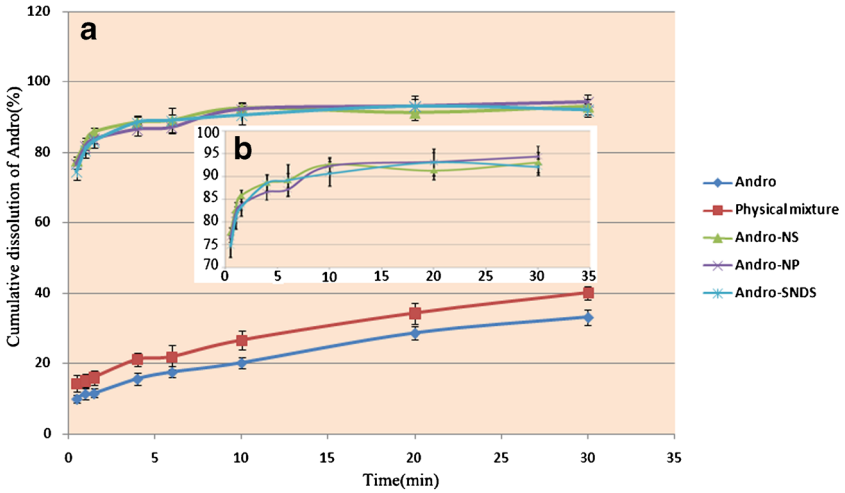

Fig. 7. (**a**) Comparison on *in vitro* dissolution of raw Andro, Andro-NS, Andro-NP, Andro-SNDS, and the physical mixture of Andro, PVPK30, and TPGS. (**b**) Magification image of *in vitro* dissolution of the Andro-NS, Andro-NP and Andro-SNDS

Powder X-ray Diffraction

Figure 6 displays the XRD diffractograms of raw Andro, the physical mixture (Andro + PVPK30 + MCC + lactose), and the spray-dried Andro-NP particles. The characteristic peak of PVPK30 was found at 11.6° and 24.1° (Fig. 6a). The characteristic peak of MCC was observed at 15.7° and 22.7° (Fig. 6b). Raw Andro exhibited characteristic crystalline peaks at 2θ of 9.9, 14.7, and 15.8° (Fig. 6c). Lactose had the characteristic crystalline peaks at 2θ of 19.9 and 33.1° (Fig. 6d). The physical mixture of Andro, MCC, PVPK30, and lactose had similar characteristic crystalline peaks compared with raw Andro, MCC, PVPK30, and lactose (Fig. 6e).

Preparation and *In Vitro* Release Evaluation of Andro-SNDS

The Andro-NP was compressed into Andro-SNDS (50 mg Andro/tablet) by direct compression technology. PVPP was used as superior disintegrant; MCC and lactose were finally used as directly compressible diluents owing to their better flowability and compressibility. The prepared Andro-SNDS complied with the required hardness (40 N) and friability (<0.1%).

Figure 7 shows that dissolution of the Andro-SNDS, Andro-NS, and spray-dried Andro-NP was superior to those of the crude powder and physical mixture in dispersion process, respectively. Within 30 min, approximate 85% of Andro was dissolved from the Andro-NP and Andro-SNDS, respectively. In contrast to this, only 31.15 and 33.37% were dissolved from the coarse Andro and physical mixture, respectively.

In Vivo Pharmacokinetics Evaluation of Andro-SNDS

Pharmacokinetic studies were performed in order to investigate whether the novel Andro-SNDS-loaded drug nanocrystal particles could improve its oral bioavailability. The plasma concentration *versus* time curves and pharmacokinetic parameters of the Andro-SNDS and the crude Andro was given in Fig. 8 and Table IV, respectively. It can be seen that Andro-SNDS possesses a fast T_{max} of 0.86 h, compared with the crude Andro that had a T_{max} of 1.47 h. The mean peak concentration of the

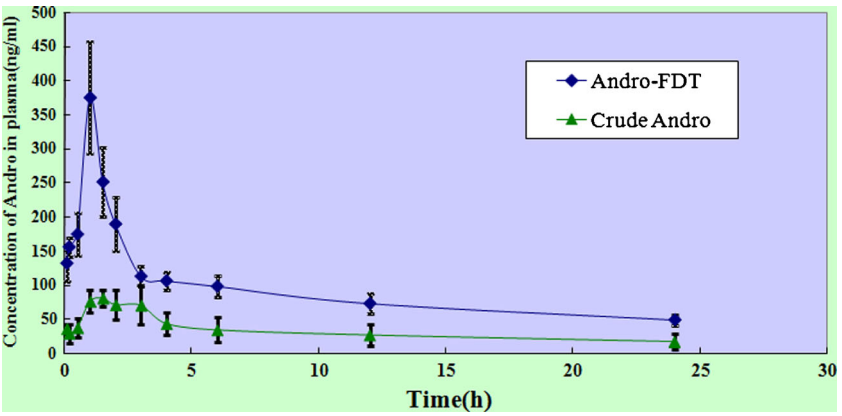

Fig. 8. Mean plasma concentration–time profiles in rats after oral administration of Andro-SNDS and the crude Andro at a dose of 10 mg/kg, respectively ($n = 6$)

Table IV. Pharmacokinetic Parameters of Andro in Rats After Oral Administration of Andro-SNDS Formulation and Crude Andro at a Dose of 10 mg/kg ($n = 6$)

Formulation	$C_{max(ng/L)}$	T_{max} (h)	$T_{1/2}$ (h)	$AUC_{(0-\infty)}$ (mg/L h)
Andro-SNDS	299.32 ± 78.54	0.86 ± 0.13	17.24 ± 2.37	4440.55 ± 764.13
Crude Andro	77.52 ± 31.73	1.47 ± 0.11	29.91 ± 4.45	1437.79 ± 354.25

Andro-SNDS andrographolide solid self-nanodispersion delivery system, *Andro* andrographolide

Andro-SNDS (299.32 ± 78.54 ng/mL) was significantly increased ($p < 0.05$), compared with that of the crude Andro (77.52 ± 31.73 ng/mL).

DISCUSSIONS

The Effect of Process Parameters on the Particle Size of Andro-NS

Preliminary screening trials were carried out for evaluating the formulation process parameters of Andro-NS (data not shown and to be published elsewhere). The results suggested that homogenization pressure, homogenization cycles, ratio of TPGS to drug, and ratio of PVPK30 to drug were key factors for production of nanosuspensions with the required stability. A Box-Behnken experimental design with 4 independent variables at 3 different levels was used to study the effects on dependent variables. Figure 2a–c shows the surface response plot of the effect of process parameters on the particle size of Andro-NS. The surface response plot of interaction homogenization pressure × cycles (Fig. 2a) showed that the particle size was attained, with the homogenization pressure between 1000 and 1200 bar. It was decreased as the power increased from 600 to 1000 bar. The particle size decreased from 2.945 to 0.557 μm with the homogenization pressure and homogenization cycles increased. And the ratio of TPGS to drug affected the particle size of BCL-NS, and the particle size decreased with the TPGS and PVPK30 amount increased (Fig. 2b, c).

The Effect of Process Parameters on the Span of Andro-NS

Figure 2d–f shows that the surface response plot of the effect of process parameters on the span of Andro-NS. Figure 2d indicates the homogenization pressure and cycle significantly affected the span of Andro-NS. The optimum homogenization pressure was between 1000 and 1200 bar, while the optimum cycles were located between 25 cycles and 30 cycles (Fig. 2d). And the minimize span might be achieved at 30 cycles and 600 bar. Furthermore, the TPGS amount as well as PVPK30 amount was not significantly affected the span of Andro-NS (Fig. 2d, f). The desirability function approach was used to find good conditions that give the minimum particle size and span (26). Figure 2g–i shows the surface-response graphs of the desirability. The optimum values of homogenization pressure, cycles, TPGS amount, and PVPK30 amount were 1000 bar, 28 cycles, 15%, and 15%, respectively.

Verification

In order to evaluate the optimization capability of the models of the Box-Behnken design, the Andro-NS were prepared according to the optimal process parameter settings that A, B, C, and D was equal to 1000 bar, 28 cycles, 15% and 15%, respectively. Table V shows that the particle size and span of Andro-NS obtained by predicted models, which demonstrated that there was a good agreement with theoretical predictions. Figure 9 demonstrated that the TEM morphology of the Andro-NS was irregular shape with a particle size of about 500nm, which demonstrated that the particles size and span of Andro-NS optimized by Box-Behnken design was satisfactory.

Effect of Matrix Formers on Redispersibility of Andro-NP During Spray-Drying

The Andro-NS was transformed into Andro-NP via spray-drying. The matrix formers were crucial for formation of spray-dried composite particles, which could prevent from the aggregation of nanocrystals due to thermal stress during drying. Therefore, the effects of different concentration of lactose and MCC on Andro-NP during spray-drying were systemically investigated. The results demonstrated that Andro-NP/MCC + lactose appeared to be more homogenous sphere-shape particles (Fig. 3c, d), compared with Andro-NP/MCC as well as Andro-NP/lactose (Fig. 3a, b). The spray-dried lactose was generally amorphous and hygroscopic (28); therefore, the Andro-NP/lactose could easily stick to the wall during spray drying process, which was unfavorable for further tabletting of Andro-SNDS. In view of these, combination of 50% concentration of MCC and lactose were used as matrix former for Andro-NP, which was able to prevent the irreversible agglomeration of the Andro nanocrystal particles during spray-drying and tabletting.

Table V. Model-Predicted and Observed Values of Particle Size and Span of Andro-NS Prepared According to the Optimal Experimental Conditions ($A = 1000$ bar, $B = 28$, $C = 15\%$, $D = 15\%$) ($n = 5$)

Dependent variable	Predicted	Observed	Bias[a]/%
Mean diameter (Y_1)	518.16 nm	509.21 nm	1.72
Span (Y_2)	1.006	1.051	−4.47

[a] Bias was calculated according to equation: Bias/% = (predicted value − observed value) / predicted value × 100%

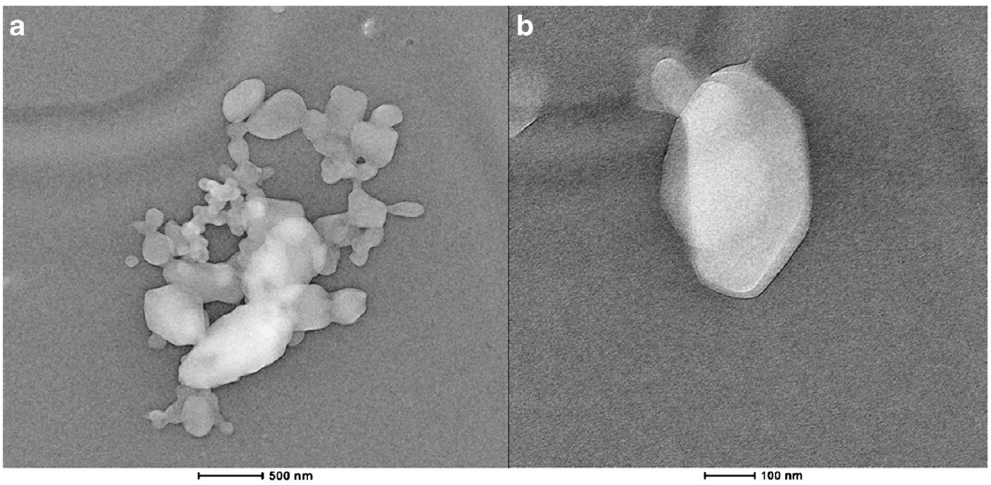

Fig. 9. Morphology of Andro-NS (**a** 500 nm; **b** 100 nm)

DSC, FT-IR, and XRD Evaluation of Andro-NP

In order to elucidate the influences of formulation processes on Andro-NP properties, the solid state of bulk Andro, the spray-dried Andro-NP, and the physical mixture was investigated using DSC, FT-IR, and XRD techniques, respectively.

DSC results of spray-dried Andro-NP demonstrated the melting peak attributable to Andro melting was shifted to 230–240°C (Fig. 4g). The slight shift in the endothermic peak of Andro-NP toward a lower temperature compared with the peak of the crude Andro (Fig. 4d) could be the result of nanoization of crystals. Reduction of the particle size and intermolecular interactions in the nanocrystals means that less energy is required to rupture the bonds between the drug molecules (29,30). Therefore, nanoparticles often exhibit left reflected in the DSC thermograms.

The FT-IR results demonstrated the absorption bands of Andro between 900 and 1800 cm^{-1} (Andro C=CH_2 and C–O–C–O–C stretchings) were still visible in the spray-dried Andro-NP (Fig. 5). Moreover, no new peaks were observed in Andro-NP. It may be the reason that the combination of Andro, PVPK30, MCC, and lactose in the spray-dried Andro-NP might be dependent of physical interaction between the two molecules, attributed to formation of Vander Waals forces or of hydrogen bond (31,32).

XRD results of the spray-dried Andro-NP demonstrated that the diffraction peaks of Andro were still maintained with decreased intensity demonstrating the presence of nanocrystals in the crystalline state (Fig. 6). The differences in peak relative intensities were probably due to the size reduction of Andro crystals and the surface adsorption of the stabilizers (33–35). Furthermore, the characterization peak of lactose in the spray-dried Andro-NP was not present at 33.1°. It was explained that partial lactose could be transformed into glassy matrix formers during spray-drying, which could prevent the Andro nanocrystals from aggregation (36,37).

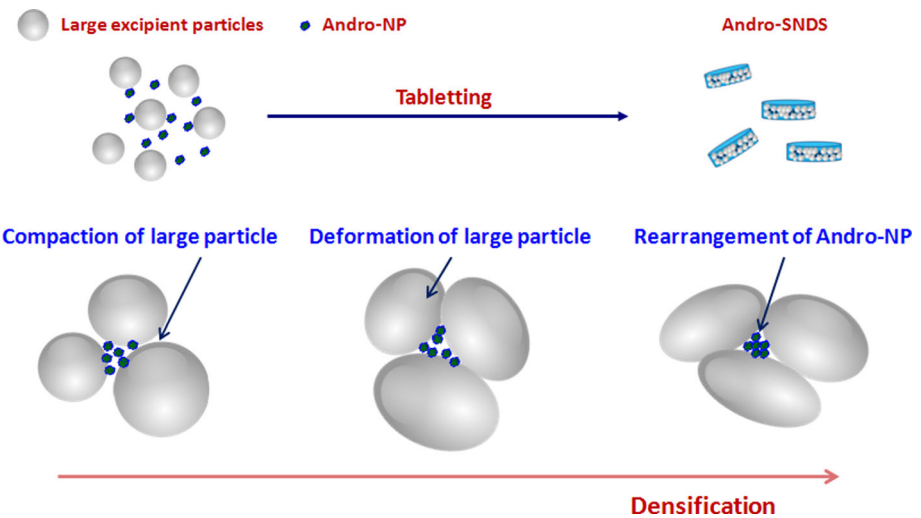

Fig. 10. Schematic image of compaction of Andro-NP in the pores between the excipient particles

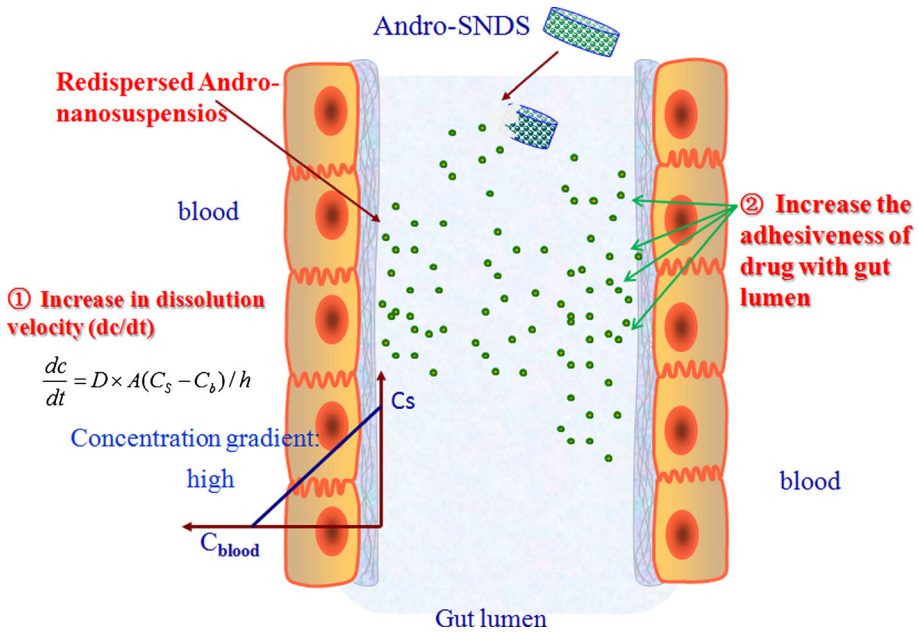

Fig. 11. Schematic image of adsorption mechanism of Andro-SNDS in gastrointestinal tract

Preparation and *in Vitro* Release Evaluation of Andro-SNDS

The Andro-NP was compressed into Andro-SNDS (dispersion tablet) by means of direct compression technology. However, the compaction of tablets is a complex powder consolidation process comprising multiple modes of volume reduction (38). In the course of tabletting, the re-dispersible Andro-NP would tend to aggregate and/or fuse together to become larger particles with reduced surface area, due to the compressive force exerted by the punches could lead to irreversible agglomeration of Andro-NP. To evaluate the success of Andro-SNDS, *in vitro* release evaluation was performed. Figure 7 demonstrated that the dissolution of the Andro-SNDS was not significantly different, compared to those of the Andro-NP and Andro-NS ($p < 0.05$). These results demonstrated that the PVPP, MCC, and lactose could help the compressed Andro-SNDS to recover back to original nanosuspensions. The redispersibility of Andro-SNDS was not comprised to a series of stresses (compression force or deformation) during tabletting. It was speculated that the MCC might be dominant for compaction of Andro-NP during tabletting. A visual representation is provided in Fig. 10; during tabletting of Andro-NP, the micronized Andro-NP could migrate into the large inter-particle pores of MCC and consolidate by virtue of particle–particle slipping and rearrangement, but Andro-NP particles could not undergo plastic deformation until they are well packed within the pores (39).

Furthermore, the dissolution of Andro-NP was significantly enhanced, which attributed to the particle size reduction and the increase of surface area of Andro nanocrystals. It can be explained by the Noyes-Whitney equation and Prandtl equation (40–42); the particle size reduction, the increase of surface area, and the decrease of diffusion distance for very small particles could enhance the dissolution velocity of the drug.

In Vivo Pharmacokinetics Evaluation of Andro-SNDS

As shown in Fig. 8, the area under the plasma concentration–time curve of the Andro-SNDS (4440.55 ± 764.13 mg/L · h) was 3.09 times ($p < 0.05$) as high as that of the crude Andro (1437.79 ± 354.25 mg/L · h). These results were consistent with those in the *in vitro* release studies (Fig. 7). As illustrated in Fig. 11, it could be the main reason that Andro-SNDS could easily reconstituted into the original Andro-NS, the reduced particle size of nanocrystals with an increase in surface area and optimization of the surface wetting by TPGS and PVPK30 significantly increased the dissolution rate of Andro, and increased the adhesiveness of gut lumen, resulting in rapid adsorption of the dissoluted Andro molecules across the gastrointestinal membrane. Furthermore, it might also be related with TPGS as inhibition of P-gp, which can could decrease the efflux mediated by P-gp and increase the oral bioavailability of drug with low solubility and/or less permeable (43–45). The in-depth mechanism behind the phenomenon is systematically elucidated in the future.

CONCLUSIONS

The novel solid self-nanodispersion delivery system-loaded Andro-nanocrystals were firstly prepared using the optimized homogenization technique followed by spray-drying and directly compression technology. TPGS and PVPK30 were chosen not only as the hydrophilic carrier but also the stabilizing agent. MCC, as well as lactose, was used as matrix former of nanocrystal composite particles and successfully prevented from Andro-NP aggregations during spray-drying and tabletting, which resulted in rapid dissolution and excellent redispersibility of Andro-SNDS. Compared with crude Andro, Andro self-nanodispersion

formulation exhibited an acceptable dissolution rate and better bioavailability.

This study developed a novel strategy to combine the features of nanocrystals and direct compression technologies to improve oral bioavailability of poorly soluble drug. The long-term stability, release, and absorption mechanism and pharmacology of Andro-SNDS will be considered in our next report. In addition, other poorly soluble drugs will be studied and evaluated by means of this combination technology in the future.

ACKNOWLEDGMENTS

The authors would like to acknowledge the support from the Scientific Research Foundation for the National Natural Science of China (No. 81560656), Fund of distinguished young scientists of Jiangxi Province and the Natural Science Fund of Jiangxi Province (No. 20161BAB205221).

COMPLIANCE WITH ETHICAL STANDARDS

Conflict of Interest The authors declare that there are no conflicts of interest.

REFERENCES

1. Lipinski CA. Drug-like properties and the causes of poor solubility and poor permeability. J Pharmacol Toxicol Methods. 2000;44:235–49.
2. Wening K, Breitkreutz J. Oral drug delivery in personalized medicine: unmet needs and novel approaches. Int J Pharm. 2011;404:1–9.
3. Sharma P, Denny WA, Garg S. Effect of wet milling process on the solid state of indomethacin and simvastatin. Int J Pharm. 2009;380:40–8.
4. Gahoi S, Jain GK, Tripathi R, Pandey SK, Anwar M, Warsi MH, *et al*. Enhanced antimalarial activity of lumefantrine nanopowder prepared by wet-milling DYNO MILL technique. Colloid Surf B. 2012;95:16–22.
5. Gebremedhin S, Singh A, Koons S, Bernt W, Konopka K, Duzgunes N. Gene delivery to carcinoma cells via novel non-viral vectors: nanoparticle tracking analysis and suicide gene therapy. Eur J Pharm Biopharm. 2014;60:72–9.
6. George M, Ghosh I. Identifying the correlation between drug/stabilizer properties and critical quality attributes (CQAs) of nanosuspension formulation prepared by wet media milling technology. Eur J Pharm Sci. 2013;48:142–52.
7. Hu X, Chen X, Zhang L, Lin X, Zhang Y, Tang X, *et al*. A combined bottom-up/top-down approach to prepare a sterile injectable nanosuspension. Int J Pharm. 2014;472:130–9.
8. Merisko-Liversidge E, Liversidge GG, Cooper ER. Nanosizing: a formulation approach for poorly-water-soluble compounds. Eur J Pharm Sci. 2003;18:113–20.
9. Keck CM, Müller RH. Drug nanocrystals of poorly soluble drugs produced by high pressure homogenisation. Eur J Pharm Biopharm. 2006;62:3–16.
10. Xiong R, Lu W, Li J, Wang P, Xu R, Chen T. Preparation and characterization of intravenously injectable nimodipine nanosuspension. Int J Pharm. 2008;350:338–43.
11. Sinha B, Müller RH, Möschwitzer JP. Bottom-up approaches for preparing drug nanocrystals:formulations and factors affecting particle size. Int J Pharm. 2013;453:126–41.
12. Peltonen L, Hirvonen J, Laaksonen T. Drug nanocrystals and nanosuspension in medicine. In: Torchilin V, editor. Handbook of nanobiomedical research, fundamentals, applications and recent developments, 1 materials for nanomedicine, vol. 3. Singapore: World Scientific; 2014. p. 169–97.
13. Van Eerdenbrugh B, Van den Mooter G, Augustijns P. Top-down production of drug nanocrystals: nanosuspension stabilization, miniaturization and transformation into solid products. Int J Pharm. 2008;364:64–75.
14. Yue PF, Li G, Dan JX, Wu ZF, Wang CH, Zhu WF, *et al*. Study on formability of solid nanosuspensions during solidification: II novel roles of freezing stress and cryoprotectant property. Int J Pharm. 2014;475:35–48.
15. Wang T, Liu B, Zhang W, Wilson B, Hong JS. Andrographolide reduces inflammation-mediated dopaminergic neurodegeneration in mesencephalic neuron-glia cultures by inhibiting microglial activation. J Pharmacol Exp Therapeut. 2004;308:975–83.
16. Shen Y, Chen C, Chiou W. Andrographolide prevents oxygen radical production by human neutrophils: possible mechanism(s) involved in its anti-inflammatory effect. Br J Pharmacol. 2002;135:399–406.
17. Rajagopal S, Kumar RA, Deevi DS, Satyanarayana C, Rajagopalan R. Andrographolide, a potential cancer therapeutic agent isolated from Andrographis paniculata. J Exp Therapeut Oncol. 2003;3:147–58.
18. Alabrese C, Berman S, Babish J, Ma X, Shinto L, Dorr M, *et al*. A phase I trial of andrographolide in HIV positive patients and normal volunteers. Phytother Res. 2000;14:333–8.
19. Coon JT, Ernst E. Andrographis paniculata in the treatment of upper respiratory tract infections: a systematic review of safety and efficacy. Planta Med. 2004;70:293–8.
20. Panossian A, Hovhannisyan A, Mamikonyan G, Abrahamian H, Hambardzumyan E, Gabrielian E, *et al*. Pharmacokinetic and oral bioavailability of andrographolide from Andrographis paniculata fixed combination Kan Jang in rats and human. Phytomedicine. 2007;7(5):351–64.
21. Ye L, Wang T, Tang L, Liu W, Yang Z, Zhou J, *et al*. Poor oral bioavailability of a promising anticancer agent andrographolide is due to extensive metabolism and efflux by P-glycoprotein. J Pharm Sci. 2011;100:5007–17.
22. Bothiraja C, Shinde MB, Rajalakshmi S, Pawar AP. Evaluation of molecular pharmaceutical and in vivo properties of spray-dried isolated andrographolide-PVP. J Pharm Pharmacol. 2009;61:1465–72.
23. Ren K, Zhang Z, Li Y, Lui J, Zhao D, Zhao Y, *et al*. Physicochemical characteristics and oral bioavailability of andrographolide complexed with hydroxypropyl-beta-cyclodextrin. Pharmazie. 2009;64:515–20.
24. Suo XB, Zhang H, Wang YQ. HPLC determination of andrographolide in rat whole blood: study on the pharmacokinetics of andrographolide incorporated in liposomes and tablets. Biomed Chromatogr. 2007;21(7):730–4.
25. Rabea P, Ahmad FJ, Iqbal Z, Samim M, Sayeed A. Solid lipid nanoparticles of anticancer drug andrographolide: formulation, in vitro and in vivo studies. Drug Dev Ind Pharm. 2014;40(9):1206–12.
26. Yue P, Li Y, Wan J, Wang Y, Yang M, Zhu WF, *et al*. Process optimization and evaluation of novel baicalin solid nanocrystals. Int J Nanomedicine. 2013;8:2961–73.
27. Zhang Y, Hu X, Liu X, Yu D, Di D, Yin T, *et al*. Dry state microcrystals stabilized by an HPMC film to improve the bioavailability of andrographolide. Int J Pharm. 2015;493:214–23.
28. Dong YC, Ng WK, Hu J, Shen SC, Tan RBH. Clay as a matrix former for spray drying of drug nanosuspensions. Int J Pharm. 2014;465:83–9.
29. Zhang D, Tan T, Gao L, Zhao W, Wang P. Preparation of azithromycin nanosuspensions by high pressure homogenization and its physicochemical characteristics studies. Drug Dev Ind Pharm. 2007;33:569–75.
30. Ng WK, Kwek JW, Yuen A, Tan CL, Tan R. Effect of milling on DSC thermogram of excipient adipic acid. AAPS PharmSciTech. 2010;11:159–67.
31. Behra A, Giri TK, Tripathi DK, Ajazuddin, Alexander A. An exhaustive review on recent advancement in pharmaceutical bioadhesive usedfor systemic drug delivery through oral mucosa for achieving maximumpharmacological response and effect. Int J Pharmaco. 2012;8:283–305.

32. Zhao GH, Kapur N, Carlin B, Selinger E, Guthrie JT. Characterisation of the interactive properties of microcrystalline cellulose-carboxymethyl cellulose hydrogels. Int J Pharm. 2011;415:95–101.
33. Yue P, Li Y, Wan J, Yang M, Zhu WF, Wang CH. Study on formability of solid nanosuspensions during nanodispersion and solidification: I. Novel role of stabilizer/drug property. Int J Pharm. 2013;454:269–77.
34. Lai F, Franceschini I, Corrias F, Sala MC, Cilurzo F, Sinico C, *et al*. Maltodextrin fast dissolving films for quercetin nanocrystal delivery. A feasibility study. Carbohydr Polym. 2015;121:217–23.
35. Dan JX, Ma YQ, Yue PF, Xie YB, Zheng Q, Hu PY, *et al*. Microcrystalline cellulose-carboxymethyl cellulose sodium as an effective dispersant for drug nanocrystals: a case study. Carbohydr Polym. 2016;136:499–506.
36. Molina MC, Armstrong TK, Zhang Y, Patel MM, Lentz YK, Anchordoquy TJ. The stability of lyophilized lipid/DNA complexes during prolonged storage. J Pharm Sci. 2004;93:2259–73.
37. Yue P, Xiao M, Xie Y, Ma Y, Guan Y, Wu Z, *et al*. The Roles of vitrification of stabilizers/matrix formers for the redispersibility of drug nanocrystals after solidification: a case study. AAPS PharmSciTech. 2015. doi:10.1208/s12249-015-0461-3.
38. Basa S, Muniyappan T, Karatgi P, Prabhu R, Pillai R. Production and in vitro characterization of solid dosage form incorporating drug nanoparticles. Drug Dev Ind Pharm. 2008;34:1209–18.
39. Koynov A, Romanski F, Cuitiño A. Effects of particle size disparity on the compaction behavior of binary mixtures of pharmaceutical powders. Powder Technol. 2013;236:5–11.
40. Xia D, Cui F, Piao HZ, Cun D, Piao H, Jiang Y, *et al*. Effect of crystal size on the in vitro dissolution and oral absorption of nitrendipinein rats. Pharm Res. 2010;27:1965–76.
41. Mauludin R, Müller RH, Keck CM. Kinetic solubility and dissolution velocity of rutin nanocrystals. Eur J Pharm Biopharm. 2009;36:502–10.
42. Muller RH, Jacobs C, Kayser O. Nanosuspensions as particulate drug formulations in therapy: rationale for development and what we can expect for the future. Adv Drug Deliv Rev. 2011;47:3–19.
43. Yu L, Bridgers A, Polli J, Vickers A, Long S, Roy A, *et al*. Vitamin E-TPGS increases absorption flux of an HIV protease inhibitor by enhancing its solubility and permeability. Pharm Res. 1999;16:1812–7.
44. Varma MV, Panchagnula R. Enhanced oral paclitaxel absorption with vitamin E-TPGS: effect on solubility and permeability in vitro, in situ and in vivo. Eur J Pharm Sci. 2005;25:445–53.
45. Guo Y, Luo J, Tan S, Otieno B, Zhang Z. The applications of vitamin E TPGS in drug delivery. Eur J Pharm Sci. 2013;49:175–86.